




# Water Resources Research®



## RESEARCH ARTICLE

10.1029/2021WR029623

## Anticipatory Drainage Base Management for Groundwater Level Optimization

D. van de Craats<sup>1</sup> , S. E. A. T. M. van der Zee<sup>1</sup> , and A. Leijnse<sup>1</sup> 

<sup>1</sup>Soil Physics and Land Management, Wageningen University & Research, Wageningen, The Netherlands

### Key Points:

- Analytical model developed for calculating time variant groundwater levels in fields with controlled drainage
- Water levels maintained closer to optimal conditions by using frequent drainage base management
- Optimal drainage base management strategy obtained based on weather forecast ensembles

### Correspondence to:

D. van de Craats,  
[daniel.vandecraats@wur.nl](mailto:daniel.vandecraats@wur.nl)

### Citation:

van de Craats, D., van der Zee, S. E. A. T. M., & Leijnse, A. (2021). Anticipatory drainage base management for groundwater level optimization. *Water Resources Research*, 57, e2021WR029623. <https://doi.org/10.1029/2021WR029623>

Received 14 JAN 2021  
Accepted 16 OCT 2021

**Abstract** Controlled drainage is normally operated on a seasonal timescale to increase availability of water and to limit nutrient loss to surface water. It is conceivable that with more frequent, or even daily, management of the drainage base, controlled drainage can be both more efficient and effective. With the analytical successive steady state model presented here, rapid simulations of groundwater level and discharge as a function of time for a field under either regular or controlled drainage are feasible. The model includes effects of sudden changes in drainage base as well as damping and attenuation of dynamics by the unsaturated zone. It is validated against a numerical model and shows good agreement with numerical results. We demonstrate how this analytical model may facilitate anticipatory drainage base management based on ensemble weather forecasts, such that groundwater levels can be maintained at a theoretical optimal level.

## 1. Introduction

Artificial drainage systems are used worldwide to remove excess water or to ascertain sufficient leaching of salts in irrigated crop lands in (semi-)arid regions (van der Molen et al., 2007). Focusing on temperate climates, considerable areas of agricultural land (roughly 10% of the rain fed agriculture) are drained via surface or subsurface measures (Smedema et al., 2004). An often used method is subsurface installation of corrugated tile drains, for example in the US and Europe (e.g., Schilling et al., 2015; Sloan et al., 2016). These drainage systems lower the field scale groundwater level, which ensures sufficient oxygen supply to crop roots, trafficability and many other benefits for crop growth optimization (Skaggs, Fausey, & Evans, 2012; Sloan et al., 2016). Agricultural production has benefitted greatly from improved drainage (Smedema et al., 2004). However, the focus regarding tile drainage in the temperate zone has also shifted toward its negative side effects such as eutrophication of surface water with N and P due to shorter groundwater travel times, changing hydrological behavior on a catchment scale and changing (aquatic) ecosystems (Ross et al., 2016; Schilling et al., 2015; Sloan et al., 2016). Also over-drainage frequently occurs, if too much water is drained from the soil during wet periods. Soil water storage is then depleted much faster during the following growing season, which results in crop water shortage (Smedema et al., 2004). The problem of over-drainage will likely become more prominent in some of the mid-latitude regions with the tendency toward drier summers, in combination with more extreme and irregular precipitation events (Rowell, 2009; Spinoni et al., 2018).

Changes to the drainage system can be adopted to limit adverse effects of artificial drainage. Instead of employing a fixed drainage base, which for a regular drainage system is the drain installation depth, the drainage base could be allowed to fluctuate by placing control structures at drainage system outlets. This allows to choose for a reduction or complete cessation of water and nutrient discharge via drains toward surface waters. This practice is referred to as controlled drainage (CD) or drain water management (DWM) (Ross et al., 2016; Skaggs, Fausey, & Evans, 2012), as opposed to free flowing, regular drainage (RD). Controlled drainage is increasingly being implemented in the US and Europe (Ross et al., 2016). An overview by Ross et al. (2016) shows that total drain water outflow is on average reduced by nearly 50% using controlled drainage (based on 17 studies in the US) as compared to regular drainage. This is in agreement with values mentioned by Skaggs, Fausey, and Evans (2012), that range from 18% to 85% reduction, as well as with values reported in several other studies (e.g., Rozemeijer et al., 2016; Sunohara et al., 2016; Williams et al., 2015). Controlled drainage thus results on average in higher groundwater levels and increased storage of water in the soil, and limits the risk of water shortage during dry periods, whilst still removing excess water in wet periods. Positive effects on crop growth are not always clearly visible and may vary from year to year with

© 2021. The Authors.

This is an open access article under the terms of the [Creative Commons Attribution](https://creativecommons.org/licenses/by/4.0/) License, which permits use, distribution and reproduction in any medium, provided the original work is properly cited.

varying atmospheric conditions, although generally crops seem to benefit from controlled drainage (Schott et al., 2017; Wang et al., 2020). However, negative side effects are known for controlled drainage as well, such as an increase in surface runoff due to these higher groundwater levels (Ross et al., 2016; Rozemeijer et al., 2016). This in turn can result in increased sediment loss and transport of particle bound nutrients and contaminants as pesticides (Bento et al., 2018; Skaggs, Fausey, & Evans, 2012; Youssef et al., 2018).

Controlled drainage is currently mostly used at a seasonal time scale, by adjusting the drainage base in view of critical moments in farm operations such as seedbed preparation, planting and harvesting (Rozemeijer et al., 2016; Skaggs, Fausey, & Evans, 2012; Sunohara et al., 2016; Williams et al., 2015). Normally the drainage base is lowered to drain depth some time before such operations to ensure good workability and trafficability, and maintained at constant, higher levels during the rest of the growing season (Skaggs, Fausey, & Evans, 2012; Williams et al., 2015). It is conceivable that efficiency of controlled drainage can be further increased with more frequent drainage base management, in anticipation on e.g., weather forecasts, crop requirements and requirements for trafficability and workability, especially when combined with real-time field measurements (Ritzema & van Loon-Steensma, 2017; van der Zee et al., 2017). In particular, this might aim at storing water when a dry period is expected and drainage of water prior to an anticipated wet period. On a regional scale, anticipating on high rainfall inputs might aid in spreading discharge over a longer time period, limiting the risk of downstream flooding.

To operate controlled drainage on this shorter time scale properly, it is imperative to estimate how the system will respond at the medium term, e.g., the following two weeks. This requires assessment of not only the response to changes in the drainage base, but also to changes in all other water balance terms, and their uncertainty. General numerical groundwater flow models such as Hydrus (e.g., Karandish et al., 2018) and SUTRA (e.g., Xin et al., 2016) have been used in drainage calculations, as well as approximate water balance models specifically focused on drainage such as DRAINMOD (Skaggs, Youssef, & Chescheir, 2012; Youssef et al., 2018). However, it requires a lot of computational effort to find an optimal drainage strategy which covers both the many possibilities to manage the drainage base (in both space and time) and also uncertainty in weather forecasts. For that reason fast (analytically based) algorithms may be favorable over more demanding numerical models.

In this study, we present an analytical model that can be used for frequent, anticipatory drainage base management. It simulates changes in groundwater level and discharge as a function of time for a field equipped with (controlled) tile drainage. We validate the model by comparing groundwater level and discharge with those from a numerical simulation model. Finally, we provide an example of how active drainage base management can aid in improving field water levels.

## 2. Methodology

### 2.1. Model Domain

The flow domain of interest is a flat agricultural field in which tile drains are present, which are separated by distance  $L$  (units: length  $[L]$ ). A conceptual sketch of a crosssection through part of this field is shown in Figure 1 (symbols are given in Appendix A). Only the domain shown here requires modeling in view of symmetry considerations, as we assume a homogeneous soil with uniformly distributed external fluxes at the lower and upper boundaries. The left ( $x = 0$ ) and right ( $x = L/2$ ) boundaries of the modeled domain are closed, as they form water divides. The upper boundary is situated at soil surface level ( $z = 0$ ), the lower at a relatively low-permeable layer at depth  $Z$   $[L]$  ( $z = -Z$ ). Precipitation  $P$  (units: length over time  $[LT^{-1}]$ ) is prescribed as a uniform flux at the upper boundary, seepage  $S$   $[LT^{-1}]$  is prescribed as uniform flux at the lower boundary. Recharge  $R$   $[LT^{-1}]$  is the uniform flux from the unsaturated zone to the groundwater, which can be different from the precipitation flux due to buffering in the unsaturated zone. All fluxes may vary in time.

The center of the drain is located at  $x = 0$ ,  $z = -D$ , where  $D$   $[L]$  is the drain depth. The drainage base ( $H_d$   $[L]$ ) is the pressure head inside the drain, and is defined with respect to the center of the drain. The drainage base can be controlled such that  $0 \leq H_d \leq D$ . We assume a circular drain envelope is present around the drain, which consists of at least the drain wall, and possibly also filter and gravel material. The drain has an inner radius  $r_i$   $[L]$  and an outer radius  $r_o$   $[L]$ , the latter consisting of drain plus envelope (Figure 1).

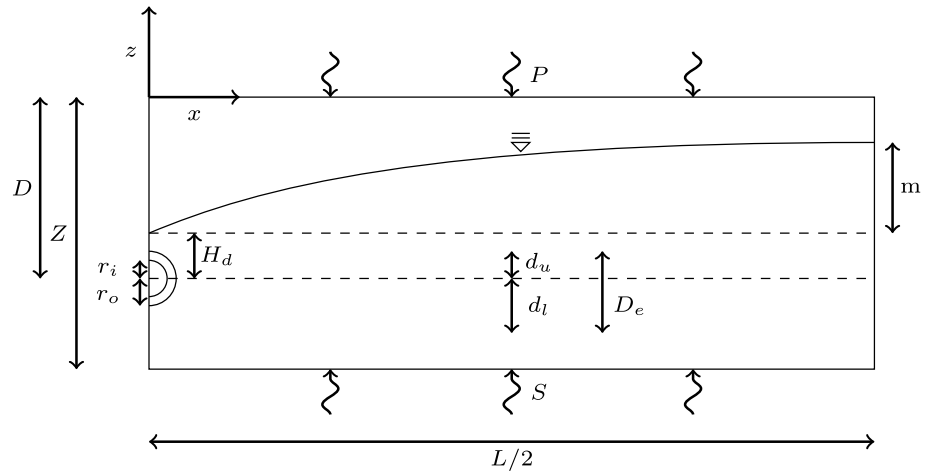


**Figure 1.** Conceptual representation of the flow domain with a tile drain on the left. The left (at the drain) and right (midway between two drains) boundaries are no flow boundaries, uniform fluxes are present at the top and bottom boundaries. An impression of the groundwater level profile is given by the curved solid line. Figure is not drawn to scale. Symbols are given in Appendix A.

## 2.2. Analytical Model

We approximate transient changes in groundwater level and drain discharge in response to changes in external forcings with a successive steady state approach. We obtain an analytical model, for which the basic equation can be solved without the need for numerical techniques. Further additions to the model, such as a time variant drainage base, recharge and specific yield, require only simple numerical techniques to be solved. This approach enables fast calculations of temporal developments, as required for frequent drainage base management.

### 2.2.1. Saturated Zone

#### 2.2.1.1. Constant Drainage Base

We take a relatively simple representation of steady state drain discharge (Hooghoudt, 1940) as point of departure for the saturated zone. Also more elaborate approximations such as those by Kirkham (1958), Ernst (1956), Ernst (1962) or Kraijenhoff van de Leur (1958) could have been used as a starting point. However, the expression of Hooghoudt (1940) works sufficiently well if we correct for the assumptions that (a) flow in the saturated zone occurs only horizontally (meaning no radial flow toward the drain), and that (b) the drain behaves like an ideal sink (Cooke et al., 2001).

Drain discharge  $Q [LT^{-1}]$  is given as function of the groundwater level difference between  $x = L/2$  and  $x = 0$  (which is our definition of head buildup,  $m [L]$ ) following Hooghoudt (1940) as

$$Q = \frac{8K_s D_e m}{L^2} + \frac{4K_s m^2}{L^2} = am + bm^2 \quad (1)$$

in which  $K_s [LT^{-1}]$  is the saturated hydraulic conductivity of the soil,  $L [L]$  the distance between two drains and  $D_e [L]$  the total equivalent flow depth, further defined in (2) and (4).  $a [T^{-1}]$  and  $b [L^{-1}T^{-1}]$  follow directly from (1). All symbols are also defined in Appendix A.

In contrast to assumption (a) in the original derivation of (1), water flows toward the drain in a radial fashion, as the drain can be considered a point sink rather than a line sink. Radial flow convergence results in increased resistance to flow, such that a higher head buildup is required to discharge the same quantity of water. The total equivalent flow depth ( $D_e$ ) is introduced in (1) to correct for (a). This parameter represents the thickness of the saturated layer through which flow would occur if water would not flow toward a point sink, but to a fully penetrating ditch extending from soil surface to the relatively low-permeable layer (providing a line sink), such that indeed only horizontal flow would occur. Hence, the total equivalent flow depth is always smaller than the real flow depth. We divide  $D_e$  into flow below and flow above drain

level. The lower equivalent flow depth  $d_l$  [L] is obtained for flow below drain level using (2), following Youngs (1985) as

$$d_l = \frac{L}{8 \left( \frac{(L - (Z - D)\sqrt{2})^2}{8(Z - D)L} + \frac{1}{\pi} \ln \left( \frac{Z - D}{r_e \sqrt{2}} \right) \right)} \quad (2)$$

in which  $r_e$  [L] is the effective drain radius. This effective drain radius accounts for the fact that the drain is not an ideal sink, assumption (b) in the derivation of (1). Water can enter the drain only through a small portion of the drain wall (at the perforations in the tube only), and the drain envelope material can become clogged with suspended soil particles or residues over time. This results in an additional resistance to flow, hence, an additional increase in required head buildup to discharge the same quantity of water.  $r_e$  is given by

$$r_e = r_i * \exp(-2\pi\alpha_e) = r_i * \exp \left[ -2\pi \left( \frac{C_d}{2\pi} \ln \left( \frac{r_o}{r_i} \right) \right) \right] \quad (3)$$

where  $r_i$  [L] and  $r_o$  [L] represent the inner and outer drain radius, respectively, and  $\alpha_e$  [-] is known as the entrance geometrical resistance factor, representing the combined effects of non-ideality and clogging (Stuyt et al., 2005).  $C_d$  [-] is the drainage resistance factor used in the numerical model, which is related to  $\alpha_e$  through (3).

If groundwater level at  $x = 0$  exceeds the drain level (which occurs when the drainage base is raised), significant saturated waterflow can occur above the drain level as well. We account for radial flow in the vertical region between the drain level and groundwater level directly above the drain by defining the upper equivalent flow depth  $d_u$  (in accordance with (2)) as

$$d_u = \frac{L}{8 \left( \frac{(L - H_0\sqrt{2})^2}{8H_0L} + \frac{1}{\pi} \ln \left( \frac{H_0}{r_e \sqrt{2}} \right) \right)} \quad (4)$$

where  $H_0$  [L] is the groundwater height at  $x = 0$ , defined with respect to drain level. The total equivalent flow depth ( $D_e$ ) is then given by summation of  $d_l$  and  $d_u$  (Figure 1). Note that radial flow is not accounted for in the remaining part of the saturated flow domain in which head buildup occurs.

We introduce the aspect of time in these equations by recognizing that a change in head buildup over time is a direct consequence of an imbalance between incoming and outgoing fluxes. With a change in head buildup, also a change in volume in the saturated zone, or more specifically a change in volume of the saturated part above  $z = -D + H_0$ , occurs. The horizontally averaged (one dimensional) volume  $V_s$  [L] (i.e., the two dimensional volume in the cross section divided by  $L/2$ ) of this part can be obtained when we describe the groundwater table profile by a quarter ellipse. We define  $V_s = \pi/4m = \bar{z}m$ , as the average of a quarter ellipse is equal to  $\pi/4$  (Appendix B). A change in  $V_s$  is related to a change in head buildup, multiplied by specific yield ( $S_y$  [-]) to correct for unsaturated zone moisture conditions:

$$\Delta V_s = S_y \bar{z} \Delta m \quad (5)$$

As a change in saturated zone volume over time is a direct consequence of an imbalance between incoming and outgoing fluxes, combining this statement with (1), yields

$$\frac{\Delta V_s}{\Delta t} = R + S - Q = R + S - (am + bm^2) \quad (6)$$

Combining (5) and (6) gives the indefinite integral

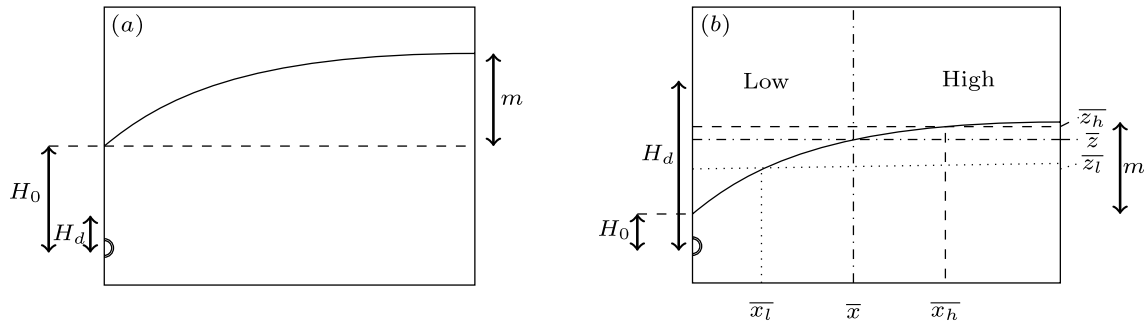


**Figure 2.** Groundwater level profiles after (a) lowering and (b) raising the drainage base, such that the pressure head inside the drain ( $H_d$ ) no longer coincides with the water level at  $x = 0$  ( $H_0$ ). In (a),  $H_0 > H_d$ , whereas in (b)  $H_0 < H_d$ . Also indicated in (b) is the position of the imaginary divide between the high and low compartments ( $\bar{x}$ ), the average groundwater level ( $\bar{z}$ ) and the average levels in the two compartments with their corresponding horizontal positions.

$$S_y \bar{z} \int \frac{1}{am + bm^2 - (R + S)} dm = \int -dt \quad (7)$$

This equation is solved, in analogy of Wesseling (1959), for the integration bounds from  $t = t$  to  $t = t + \Delta t$ , and  $m = m(t)$  to  $m = m(t + \Delta t)$  to obtain the change in head buildup over time (see Appendix B for details) as

$$m(t + \Delta t) = \frac{AB + A^2 \tanh\left(\frac{2A}{\pi S_y} \Delta t\right)}{2b \left( B \tanh\left(\frac{2A}{\pi S_y} \Delta t\right) \right)} - D_e \quad (8)$$

where  $A = \sqrt{a^2 + 4b(R + S)} [T^{-1}]$  and  $B = 2bm(t) + a [T^{-1}]$ . We assume that  $D_e$ ,  $S_y$  and boundary fluxes are constant in time in the derivation of (8). The error introduced by this assumption can be limited by taking time step  $\Delta t$  such that changes in  $D_e$  and  $S_y$  are small. In case of a steady precipitation and seepage rate, (8) tends to the steady state head buildup (1), whereas if time variant boundary fluxes are prescribed, a steady state situation in (8) is never reached. Note that drain discharge follows directly from (1) for the obtained head buildup in (8).

### 2.2.1.2. Lowering the Drainage Base

Thus far, we have only considered controlled drainage by increasing the total equivalent flow depth by  $d_u$  (4) when the water level directly above the drain exceeded drain level. However, controlled drainage allows lowering or raising of the drainage base over time. In case the drainage base is lowered at some time  $t$ ,  $H_0$  exceeds the drainage base,  $H_d$ . This situation, shown in Figure 2a, leads to additional discharge of water. We approximate this additional discharge by dividing the water level (and thus discharge) response into a response due to (a) head buildup resulting from an excess in incoming fluxes (as discussed in the previous section) and (b) a head difference due to lowering of  $H_d$ . This first driving force (a) is modeled as before, with  $m(t = t)$  being equal to the head buildup immediately before lowering of  $H_d$ . The second driving force (b) is modeled with  $m_0(t = t) = \Delta H_d [L]$  substituted for  $m$  in (8), i.e., the initial head buildup  $m_0$  is equal to the change in drainage base. Recharge and seepage only affect (a), such that for (b),  $A = a$  in (8).  $m_0$  tends to zero over time, resulting in a diminishing contribution of (b) to water level and discharge dynamics over time, as  $H_0$  tends to  $H_d$ .

The second driving force requires two additional changes in (8). The total equivalent flow depth for (b) is reduced by recalculating  $d_u$  using  $H_d$  rather than  $H_0$  in (4), and the discharge due to (b) is multiplied with  $4/\pi$ . The latter is required as we implicitly assume that the water table for (b) is elliptical, giving a one dimensional volume of  $\pi/4 m_0$ , whereas the actual one dimensional volume equals  $m_0$ .

### 2.2.1.3. Raising the Drainage Base

When the drainage base is raised at some time  $t$ ,  $H_d$  exceeds  $H_0$  and drain discharge ceases. The drain boundary becomes inactive as we do not consider sub-irrigation. This situation is shown in Figure 2b. The groundwater table flattens toward its average height, such that head buildup  $m$  and water level above the drain  $H_0$  tend to 0 and  $H_0(t = t) + \bar{z}m(t = t)$ , respectively. Recharge and seepage do not influence head buildup  $m$ , but rather they impact the overall groundwater level uniformly. Hence, the contribution of recharge and seepage is simply added to  $H_0$ , whilst accounting for  $S_y$ .

We approximate flattening of the groundwater table over time by envisioning two zones, a lower and a higher zone shown in Figure 2b. These zones are (imaginarily) separated at horizontal position  $\bar{x}L/2 = \left(1 - \sqrt{1 - (\pi/4)^2}\right)L/2$ , where the groundwater level equals the average groundwater level (Appendix B). Water levels in the lower zone will increase, whereas water levels in the higher zone will decrease toward the average height ( $\bar{z}m$ ) as the excess volume with regard to the average level in the upper zone equals the shortage of water in the lower zone. We assume the elliptical groundwater table profile remains intact during the period of flattening, such that the definitions of  $\bar{x}$  and  $\bar{z}$  remain intact.

We identify (Appendix B) an average water level  $\bar{z}_l m [L]$  and  $\bar{z}_h m [L]$  for the lower and upper zones, respectively, with their respective horizontal positions  $\bar{x}_l L/2 [L]$  and  $\bar{x}_h L/2 [L]$ . We assume that flow from the higher zone to the lower zone can be described by a Darcy flux, such that

$$Q_l = -K_s D_s \frac{(\bar{z}_h - \bar{z}_l)m}{(\bar{x}_h - \bar{x}_l) \left(\frac{L}{2}\right)} \quad (9)$$

where  $Q_l [L^2 T^{-1}]$  is the leveling flux from the high to the low zone and  $D_s [L]$  gives the average saturated zone thickness, given by  $(Z - D + H_0 + \bar{z}m)$ . The use of the total equivalent flow depth is not required here since flow is now mainly horizontal (no radial flow toward the drain). We rewrite (9) (Appendix B for details) as we are not specifically interested in this leveling flux, but rather in the effect of this flux on  $H_0$  and  $m$ . We specify a two dimensional volume  $V_l [L^2]$  and change in volume over time for the lower zone, which read

$$\Delta V_l = S_y \bar{x} \left(\frac{L}{2}\right) m \Delta \bar{z}_l; \quad \frac{\Delta V_l}{\Delta t} = Q_l \quad (10)$$

Combination of (9) and (10), substitution of  $\bar{z}_l^* [-]$  (given by  $\bar{z}_l^* = \bar{z}_l - \bar{z}$ ) for  $\bar{z}_l$  and integration from  $t = t$  to  $t = t + \Delta t$  and from  $\bar{z}_l^* = \bar{z}_l^*(t)$  to  $\bar{z}_l^* = \bar{z}_l^*(t + \Delta t)$  yields

$$\bar{z}_l^*(t + \Delta t) = \bar{z}_l^*(t) * \exp \left[ \frac{K_s D_s \Delta t}{S_y \left(\frac{L}{2}\right)^2 (\bar{x}_h - \bar{x}_l)} \frac{\pi(1 - \bar{x}) - 4 \sin^{-1}(1 - \bar{x})}{-\bar{x}(1 - \bar{x})(\pi(1 - \bar{x}) - 4 \cos^{-1}(1 - \bar{x}))} \right] \quad (11)$$

A change in water height of the lower compartment is translated into a change in  $m$  and  $H_0$ , given the assumed elliptical shape, such that

$$m(t + \Delta t) = m(t) \frac{-8\bar{x} \bar{z}_l^*(t + \Delta t)}{4 \sin^{-1}(1 - \bar{x}) - \pi(1 - \bar{x})}; \quad H_0(t + \Delta t) = H_0(t) + \bar{z}(m(t) - m(t + \Delta t)) \quad (12)$$

### 2.2.2. Unsaturated Zone

To model transient groundwater levels more accurately we need to include both the saturated and the unsaturated zone as the unsaturated zone buffers precipitation and influences the relation between storage change



and water level change. These two effects are reflected in specific yield and the transformation of precipitation to recharge. We assume that both recharge and specific yield are uniform across the horizontal domain, and that their values obtained at  $x = \bar{x}L/2$  are a good indicator of their average values over the horizontal domain. Specific yield in an unsaturated zone in hydrostatic equilibrium is (Appels et al., 2017)

$$S_y = \frac{\partial V_u}{\partial z_u} = (\theta_s - \theta_r) \frac{(\alpha D_u)^n - \left( (\alpha D_u)^n + 1 \right)^{\frac{1}{n}} + 1}{(\alpha D_u)^n + 1} \quad (13)$$

where  $V_u [L]$  denotes the volume of drainable water in the unsaturated zone,  $D_u [L]$  the average thickness of the unsaturated zone,  $z_u [L]$  the unsaturated zone coordinate, zero at the level of the groundwater and positive upward,  $\theta_s [L^3 L^{-3}]$  the soil water content at saturation,  $\theta_r [L^3 L^{-3}]$  the residual water content and  $\alpha [L^{-1}]$  and  $n [-]$  the Van Genuchten fitting parameters, following van Genuchten (1980).

Instead of a hydrostatic equilibrium in the unsaturated zone (as in (13)), we assume the internal flux rate in the unsaturated zone to be constant with depth, but not necessarily zero. Hence, the internal flux rate is equal to recharge rate, and precipitation is divided instantaneously throughout the unsaturated zone, ignoring infiltration fronts. We therefore combine the Darcy equation for vertical flow (describing flux as function of both head gradient and hydraulic conductivity) with the van Genuchten (1980) functions (describing hydraulic conductivity and water content as function of pressure head) to yield (see Appendix B for details)

$$dh_u = \frac{R - K_s \left( 1 + (\alpha |h_u|)^n \right)^{\frac{1-n}{2n}} \left( 1 - \left( 1 - \frac{1}{1 + (\alpha |h_u|)^n} \right)^{\frac{n-1}{n}} \right)^2}{K_s \left( 1 + (\alpha |h_u|)^n \right)^{\frac{1-n}{2n}} \left( 1 - \left( 1 - \frac{1}{1 + (\alpha |h_u|)^n} \right)^{\frac{n-1}{n}} \right)^2} dz_u \quad (14)$$

where  $K_s [LT^{-1}]$  is the saturated hydraulic conductivity,  $R [LT^{-1}]$  is the recharge rate to the saturated zone (defined positive downward, i.e., into the saturated zone) and  $h_u [L]$  is the pressure head in the unsaturated zone at a given location  $z_u$ . Equation 14 is solved numerically as a solution cannot be readily obtained for a non-zero recharge rate. To do so the soil is divided into equally sized compartments with size  $dz_u [L]$  from groundwater to field surface level. As specific yield is based on water volumes rather than pressure heads (13), pressure heads in (14) are translated to water contents (van Genuchten, 1980) as

$$\theta_h = \theta_r + (\theta_s - \theta_r) \left( 1 + (\alpha |h_u|)^n \right)^{\frac{1-n}{n}} \quad (15)$$

where  $\theta_h [L^3 L^{-3}]$  is the water content given pressure head  $h_u$ . Summation over the entire unsaturated zone gives the one dimensional volume of drainable water in a vertical column of the unsaturated zone,  $V_u [L]$ . From this we obtain specific yield  $S_y$  as

$$S_y = \theta_s + \frac{dV_u}{dz_u} = \theta_s + \frac{1}{2dz_u} \left( \sum_{z_u=0}^{D_u-dz_u} \theta_h dz_u - \sum_{z_u=0}^{D_u+dz_u} \theta_h dz_u \right) \quad (16)$$

In this expression,  $dV_u/dz_u [LL^{-1}]$  is the change in drainable water in the unsaturated zone with a change in unsaturated zone thickness of  $2dz_u$ , a numerical approximation of the definition used in (13).

Finally, we consider the water balance of the unsaturated zone to couple the unsaturated zone to the saturated zone. Its volume is obtained by summation of water contents (15) over the entire zone. The change in water volume during a given time step equals precipitation minus recharge plus the change in volume due to a change in groundwater level, which effectively changes the thickness of the unsaturated zone. We

**Table 1**  
Range of Parameter Values Out of Which Values for Each Simulation in the Scenario Analyses Are Obtained

Parameter	Unit	Minimum	Maximum	Scenario
$L$	$m$	4	20	1–3
$D$	$m$	0.5	1.2	1–3
$\alpha_e$	-	$\log(0.05)$	$\log(1)$	1–3
$P$	$md^{-1}$	$1e-04$	0.002	1–3
$P_w$	$md^{-1}$	$2e-04$	0.0021	1
$H_d$	$m$	0.05	0.45	1,3
$H_d$	$m$	$0.1*H_{dw}$	$0.9*H_{dw}$	2
$H_{dw}$	$m$	0.05	0.45	1–2
$H_{dw}$	$m$	$0.1*H_d$	$0.9*H_d$	3

Note. Column 'Scenario' denotes for which scenario the parameter range is used. Values for  $\alpha_e$  are picked on a log10 scale. Subscript 'w' denotes that parameter values are chosen from a different range during the warmup period (i.e. to obtain the initial steady state).

obtain the recharge rate for a following time step by iteratively solving (14), for a known unsaturated zone water volume and thickness.

### 2.3. Numerical Model

We also simulate water flow using SUTRA v2.2 (Voss & Provost, 2002), a numerical finite element model for saturated-unsaturated groundwater flow, to compare our analytical model with. The relation between water content, pressure and hydraulic conductivity used in SUTRA is given by the Van Genuchten functions (van Genuchten, 1980). The required quadrilateral mesh is created using GMSH (Geuzaine & Remacle, 2009). We explicitly include the drain in this mesh, and refine the mesh around the drain to accommodate relatively high flow velocities and flow line curvature in this region.

The drain boundary is modeled by a series of fixed pressure nodes for which we specify a pressure head inside the drain (i.e., the drainage base). We apply changes in the drainage base by either adjusting the pressure assigned to the drain nodes when the groundwater level at  $x = 0$  is equal to or higher than the drainage base, or by inactivating the nodes if the water level falls below the drainage base. The drain envelope, i.e., the region between  $r_i$  and  $r_o$  (Figure 1), is given a smaller hydraulic conductivity relative to the surrounding soil, given by  $K_e = K_s/C_d [LT^{-1}]$ , where  $K_s [LT^{-1}]$  is the saturated hydraulic conductivity of the soil and  $C_d [-]$  is the drainage resistance factor. This factor is related to the entrance geometrical resistance factor  $\alpha_e$ , as given in (3). Cases where the groundwater level rises above soil surface were excluded in this paper as with SUTRA overland flow is not accounted for.

### 2.4. Model Validation

We compare three sets of simulation results (referred to as scenarios), detailed below, to validate the behavior of the analytical model. We consider a silty loam soil, with  $K_s = 0.108 md^{-1}$ ,  $\theta_r = 0.067$ ,  $\theta_s = 0.45$ ,  $\alpha = 2.0 m^{-1}$  and  $n = 1.41$ . The inner- and outer drain radius are 0.03 and 0.04 m, respectively, for all scenarios, and the seepage rate is a constant  $0.1 mmd^{-1}$ . Also aquifer thickness ( $Z$ ) is fixed, at 2 m. Other parameters are obtained in the range provided in Table 1 using Morris trajectories (Campolongo et al., 2007; Morris, 1991), which ensures that parameter combinations over the whole defined parameter space are used, albeit in discrete steps. As starting point for each simulation, a steady state condition for a given set of parameters is obtained, after which one of the parameters is altered to follow the transient behavior toward a new steady state. Precipitation is either raised or lowered in 168 individual simulations in scenario 1. The drainage base is lowered in 83 simulations in scenario 2, and the drainage base is raised in scenario 3 for an equal number of simulations. As some of the parameter combinations result in groundwater levels rising above soil surface (which are discarded), the effective number of simulations used in the scenario analyses is slightly less.

In addition to the scenarios, we also simulate a hypothetical real world case for one drainage system over a six month period (01-07-2018 to 31-12-2018), using both the analytical and numerical model. We use hourly precipitation data recorded at Schiphol Airport, the Netherlands (KNMI, 2019) as input for rainfall. The precipitation rate is reduced to  $K_s$  in case it exceeds the maximum infiltration rate  $K_s$ , and the remaining water is lost to surface runoff instantaneously. Drainage base management is applied based on trial and error to roughly maintain groundwater levels between 0.6 and 1.0 m below soil surface. The field under consideration has a drain spacing of 10 m, drain depth of 1.2 m and total aquifer thickness of 2.5 m. The entrance geometrical resistance factor is set at 0.1. All other parameters are the same as for the scenarios.



### 2.5. Model Application

A situation in which the analytical model can be particularly useful is a situation in which frequent anticipatory drainage base management is based on current and near future conditions. We give an example of such a situation for the same field as described above, but restrict the maximum rise in drainage base to 0.3 m above drain level. Starting on October 25th, 2018, we look 16 days ahead using the ensemble weather forecast provided by the Global Ensemble Forecast System v11 (Zhou et al., 2017), which consists of 21 simulations providing (amongst others) precipitation with a 3–6 hr timestep on a  $0.5^\circ$  grid. In this case we use precipitation data obtained at  $52.0^\circ\text{N}$ ,  $4.5^\circ\text{E}$ , which roughly coincides with the location of Schiphol Airport, so that we can compare the forecast to the actual rainfall observations at this weather station. However, note that we did not process the forecasts (e.g., no downscaling), which would be necessary for normal use.

For this example we define an optimal range between which we want the water levels midway between the drains to be. This range is set between 0.7 and 0.8 m below soil surface, with an optimum of 0.75 m. Simulated water levels will unavoidably move outside this range in dry or wet situations. Drainage base management is then aimed at restoring water levels to values within these bounds as quickly as possible. We use the following approach to find a good management strategy for the near future, using only the analytical model.

1. We calculate the expected groundwater level development for each of the 21 available weather forecasts, using a constant drainage base in time, yielding 21 base simulations. We determine if and when water levels exceed the upper limit of the optimal range for each simulation. Many possibilities now exist as to how the drainage base could be adapted to avoid or limit this exceedance, both in time (when to change the drainage base) and space (by how much to change the drainage base). Here we use discrete steps of when and how the drainage base can be changed, with time steps of 6 hr, and height differences of 5 cm
2. When at a certain moment in time the groundwater level exceeds the upper limit, we apply all relevant changes in drainage base at all possible times prior to this exceedance, and calculate the resulting groundwater levels for each of these options. The unsaturated zone is now neglected, and specific yield and recharge as obtained for the base simulation are used to speed up the calculations.
3. We obtain the five management options which perform best for each of the original weather forecasts. As criterium for 'best', we first calculate the squared difference between modeled and optimal groundwater level (i.e., 0.75 m below soil surface) for those points that fall outside the optimal range, multiply it with an exponentially decreasing weight function with time to give more importance to water levels in the near future, and then sum these data points. The weight function is introduced as both uncertainty in weather forecasts increases with time, and the further away in future, the more time is left for timely intervention in the drainage base if necessary.
4. For these five management options we calculate when the drainage base should be raised again in order to avoid over-drainage. This point is chosen when water levels are at their optimal level. The development of the water levels is recalculated with this raised drainage base. Steps (2), (3) and (4) are repeated if the groundwater level exceeds the upper limit again, which can occur in case of multiple rain events. This procedure is followed until no better management option can be found for a given forecasts, and the most optimal option is selected.
5. Finally, we obtain the median of the best management options for each of the 21 weather forecasts, which we claim to be the optimal strategy. We forecast groundwater level and discharge development over time using this strategy for each individual weather forecast to obtain an idea of the influence of weather forecast uncertainty.

## 3. Results

The analytical and numerical models produce a similar steady state head buildup (Figure 3a). On average the analytical model simulates a slightly higher head buildup, exceeding the numerical model result by  $0.6 \text{ cm} \pm 2.0 \text{ cm}$  (based on 544 data points, and  $\pm 2.0$  denoting one standard deviation). The relative difference, obtained for each individual data point as analytical minus numerical, divided by the numerical result, equals  $6.3\% \pm 22.2\%$ . The largest percentual deviations occur in the lower ranges of  $m$  (Figure 3a), but these are limited in absolute size, whereas the largest absolute deviations occur for a larger head buildup. We consider such deviations acceptable in view of uncertainty related with heterogeneity of soil hydraulic

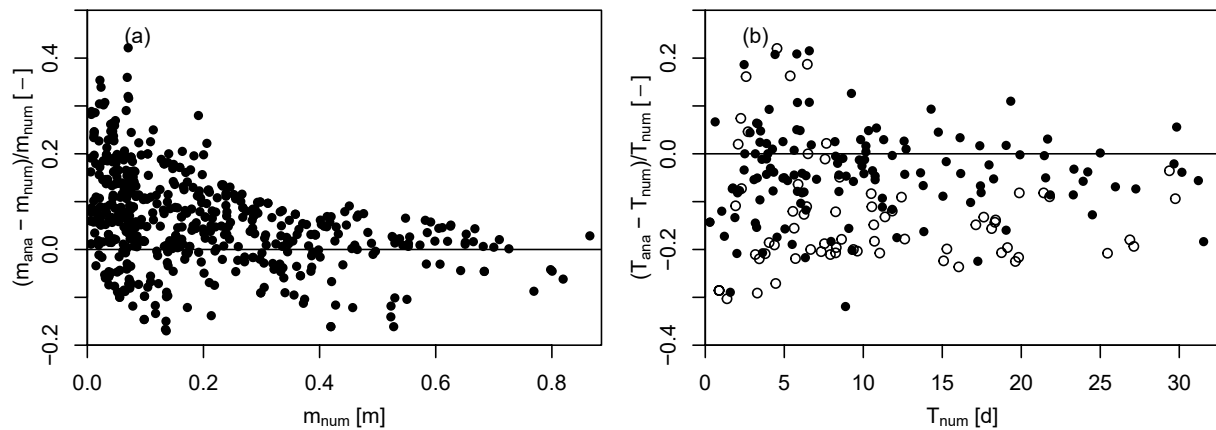


**Figure 3.** Relative differences of (a) analytical head buildup ( $m_{\text{ana}}$ ) with respect to numerical results ( $m_{\text{num}}$ ) for steady state solutions, before and after changing precipitation rate or drainage base and (b) analytical response time ( $T_{\text{ana}}$ ) with respect to numerical response time ( $T_{\text{num}}$ ) for solutions with a change in precipitation rate (solid symbols) or lowering of drainage base (open symbols).

conductivity or functioning of the drains (present in our model as  $\alpha_e$ ). We conclude that (1) to (4) can adequately predict steady state groundwater levels midway between the drains for controlled drainage systems.

Larger deviations between numerical and analytical results are obtained for situations with poorly functioning drains, where the entrance geometrical resistance factor exceeds one ( $\alpha_e > 1$ , results not shown). In these instances, the numerical model simulates heads at  $x = 0$  which significantly exceed those inside the drain, owing to the larger head gradients required for water to enter the drains. As a head difference inside and directly above the drain in a steady state condition is not allowed in the analytical model, the analytical and numerical model represent the same situation very differently, resulting in e.g., differences in flow depth and thus head buildup. Hence, we limit the model to situation where  $\alpha_e < 1$ .

Response times following changes in precipitation rate and lowering of the drainage base (Figure 3b) are obtained as the time required for  $m$  to reach  $1/e$  times the total change in  $m$ . In case of a change in precipitation rate, the response time is only slightly lower for the analytical model as compared to the numerical model ( $-0.4 \text{ d} \pm 1.1 \text{ d}$ , based on 136 data points), which corresponds to a relative difference of  $-4.0\% \pm 11.1\%$ . Buffering in the unsaturated zone proves to be crucial in modeling a correct response time. If neglected (hence reducing (14) to  $dh_u = -dz_u$ , results not shown), response times of the groundwater system upon changes in recharge rate are severely underestimated analytically, even for these shallow unsaturated zones. As we do not consider infiltration fronts, but divide precipitation evenly over the unsaturated zone, the analytical model may still slightly underestimate response times.

The difference in response time upon lowering of the drainage base (scenario 2) is somewhat larger, with the analytical response being faster than the numerical one ( $-1.6 \text{ d} \pm 1.5 \text{ d}$ , based on 69 data points), which corresponds to a relative difference of  $-13.2\% \pm 11.2\%$ . A reason for this difference is that, in contrast to the numerical model, we assume an immediate and proportional response along the entire groundwater profile in the analytical model, whereas in reality water levels close to the drain will drop first, only then followed by a response midway between the drain. For similar reasons the initial discharge upon lowering of the drainage base is mostly lower in the analytical model (open symbols Figure 4a) as well. Initially the main driving force for discharge is a difference in pressure head between drain and groundwater immediately above the drain, rather than the difference between drain and groundwater midway between the drains, as assumed in the analytical model. However, the two models agree much better after 24 hr (solid symbols in Figure 4a). For the remaining period, discharge in the analytical model generally slightly exceeds discharge calculated by the numerical model, as the total drained volumes by both models must be (nearly) equal.

When raising the drainage base (scenario 3), discharge stops until  $H_0$  reaches  $H_d$ . The time required for this to happen is given in Figure 4b. The number of points in this figure is limited (22 points only), as in the numerical model in 45 instances the water level at  $x = 0$  exceeds  $H_d$  even after raising the drainage base. This occurs mostly when the raise in drainage base is small (a few centimeters), or when the entrance resistance

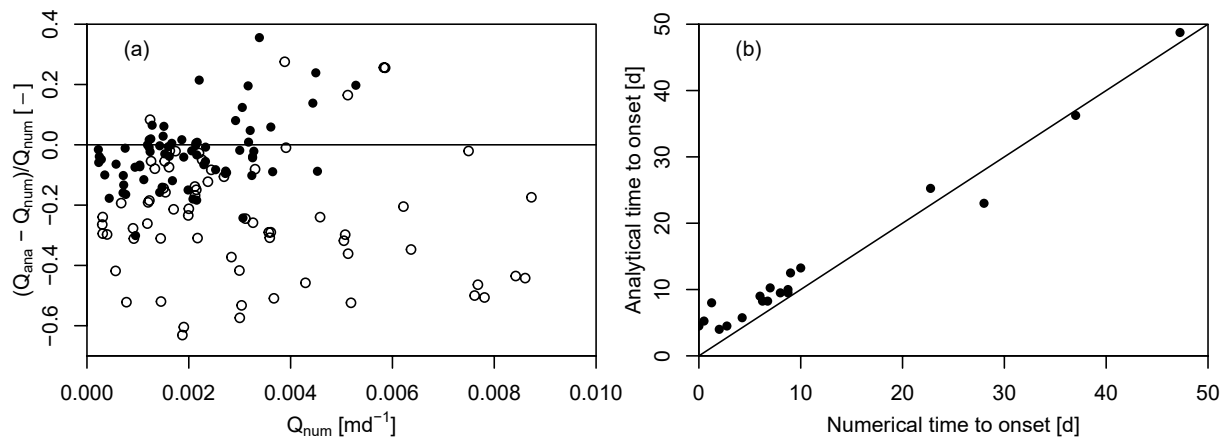


**Figure 4.** (a) Relative difference of analytical discharge ( $Q_{ana}$ ) with respect to numerical discharge ( $Q_{num}$ ), following a decrease in drainage base. Open symbols indicate initial discharge, two minutes after lowering the drainage base, solid symbols indicate discharge after 24 hr. (b) Time to onset of discharge after raising the drainage base, for the analytical model compared to the numerical model.

of the drain is large (close to 1), in combination with a large head buildup. The reason for this is that the head at  $x = 0$  in the analytical model is (in steady state situations) per definition equal to  $H_d$ , whereas this restriction is absent in the numerical model. For these 45 instances, the analytical model mostly resumes discharge soon after raising the drainage base, with a median time required of only 6 hr.

The time required for discharge to recommence for the simulations shown in Figure 4b is larger in the analytical model, and exceeds the numerical results by  $1.9 \text{ d} \pm 2.3 \text{ d}$ . This difference is both due to the slightly higher head at  $x = 0$  in the numerical model in steady state, and due to the assumption that the water table shape remains elliptical. In contrast to this assumption, water levels at  $x = 0$  rise more rapidly in the numerical model such that the shape of the water table changes from elliptical to more of an error function shape. The overall effect of this disagreement between the models on analytical model performance is limited. Head buildup midway between the drains is normally mostly small compared to changes in the drainage base, such that not groundwater leveling, but rather the incoming fluxes of recharge and seepage are the main driving mechanisms for raising water levels and restoring discharge. In addition, discharge rates after recommencing of drain flow due to leveling of the groundwater table will be small due to the limited remaining head buildup.

Figure 5a shows the development of the water levels over time for the hypothetical real world case. Water levels midway between the drain obtained by the analytical model (solid black line) correspond well to those obtained numerically (dashed blue line) for most of the period, and both models respond to precipitation events (black bars) and changes in the drainage base (red solid line) in a logical way. The agreement between the numerical and analytical model is good, with a mean absolute error (MAE) of 0.023 m and root mean squared error (RMSE) of 0.048 m. The Nash-Sutcliffe Efficiency (NSE), ranging from minus infinity to 1, equals 0.80.

Water levels are slightly higher in the analytical model for most of the period, in correspondence with higher steady state water levels (Figure 3a). Water levels are considerably higher in the analytical model than the numerical model around day 70, with significant precipitation (57 mm within three days). Despite limiting precipitation rates to  $K_s$  (and attributing the rest to surface runoff), not all precipitation actually infiltrates in the soil in the numerical model due to limitations in infiltration capacity in the unsaturated zone. This reduces the water level response for this particular event in the numerical model. Responses in water level upon precipitation are well comparable between both models for all other situations, although an increase in water level occurs slightly (a few hours) sooner in the analytical model than in the numerical model. This is likely a consequence of spreading precipitation evenly throughout the unsaturated zone. The effects of lowering and raising of the drainage base on water levels midway between the drains is also well comparable between both models.

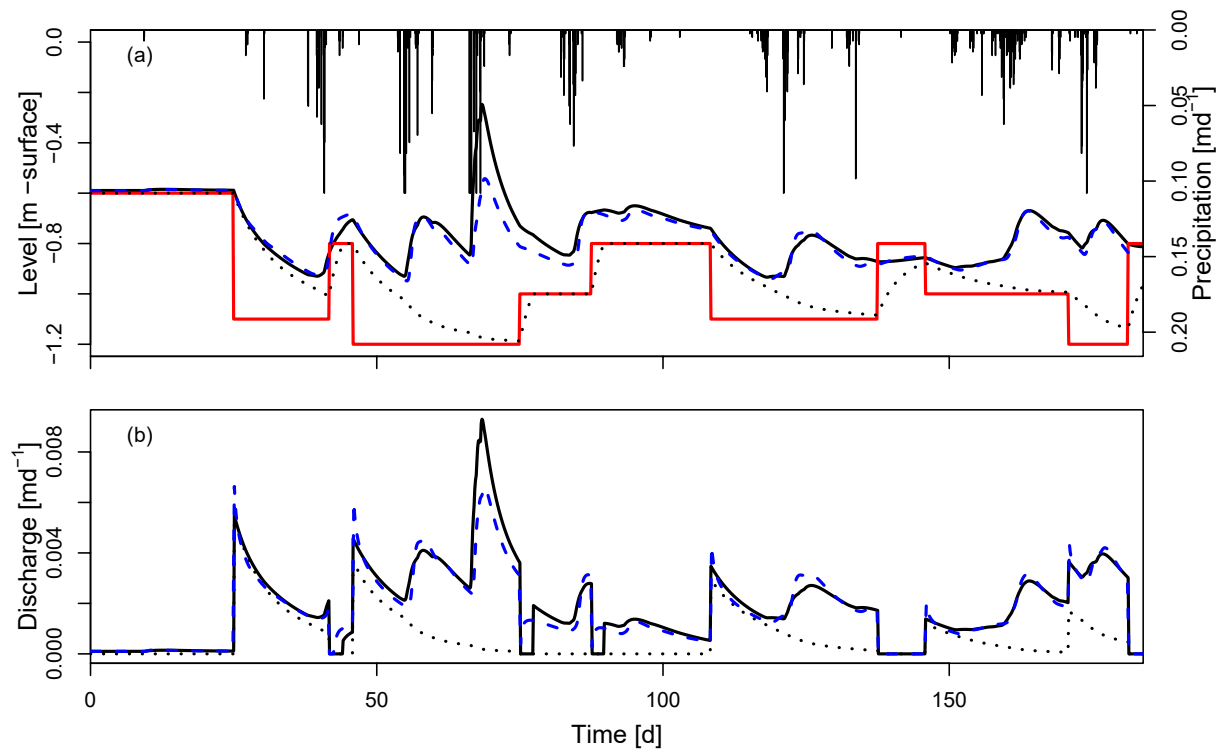


**Figure 5.** (a) Modeled water levels midway between the drains with respect to field surface over a period of six months, for the numerical model (blue dashed) and the analytical model (black). For the analytical model, the water level at  $x = 0$  is also given (dotted line). Water levels respond to precipitation (vertical bars, right axis) and changes in drainage base (red solid line). (b) Modeled drain discharge over the same period as (a), with color - and pattern indications similar as in (a).

Discharge (Figure 5b) in the analytical model (solid black line) corresponds well to the numerical model (dashed blue line) for most of the period, with a MAE of  $0.24 \text{ mmd}^{-1}$ , RMSE of  $0.46 \text{ mmd}^{-1}$  and NSE of 0.89. Peak discharge following a rainfall event is slightly lower in the analytical model as compared to the numerical model, except for the event around day 70, for reasons discussed above. Peak discharge after lowering the drainage base is comparable between both models, although the initial peak is somewhat lower in the analytical model, as seen in Figure 4b as well. Discharge some days after lowering the drainage base is again slightly higher in the analytical model. As observed in scenario 3, periods without discharge after raising the drainage base last longer in the analytical model. This is clearly visible around day 40 (Figure 5b). Also, in some instances (around day 80 and 90), a raise in drainage base does not stop discharge in the numerical model, whereas it takes approximately two days in the analytical model to recommence. This coincides with water levels at  $x = 0$  being below the drainage base (dotted black line in Figure 5a) in the analytical model.

Finally, we move to the application example, given in Figure 6. The covered time period coincides approximately with days 110–125 in the hypothetical real world case (Figure 5). The period prior to this event was quite dry, hence the initial drainage base is set relatively high, and initial head buildup is small. The calculated heads of the base simulations, with the drainage base fixed at its original height of 0.3 m above drain level, are shown in Figure 6a by the red areas and lines. The median (solid line), 50th percentile (dark shaded) and extremes (light shaded) are given, based on 21 weather forecasts given in Figure 6b. The expected water levels rise toward the soils surface around day six for some of the forecasts, and, in 75% of the forecasts, remain above the optimal range (indicated by dot-dashed lines) for the remaining ten day period. Even for the driest forecasts the water levels midway between the drains remain around the upper limit of the optimal range. Drainage base management is therefore required to limit lengthy periods with water levels exceeding the optimal range.

The optimal management strategy for each weather forecasts is obtained, and the median and 50th percentile of these solutions are given in Figure 6a by the dashed black line and gray shaded area, respectively. A

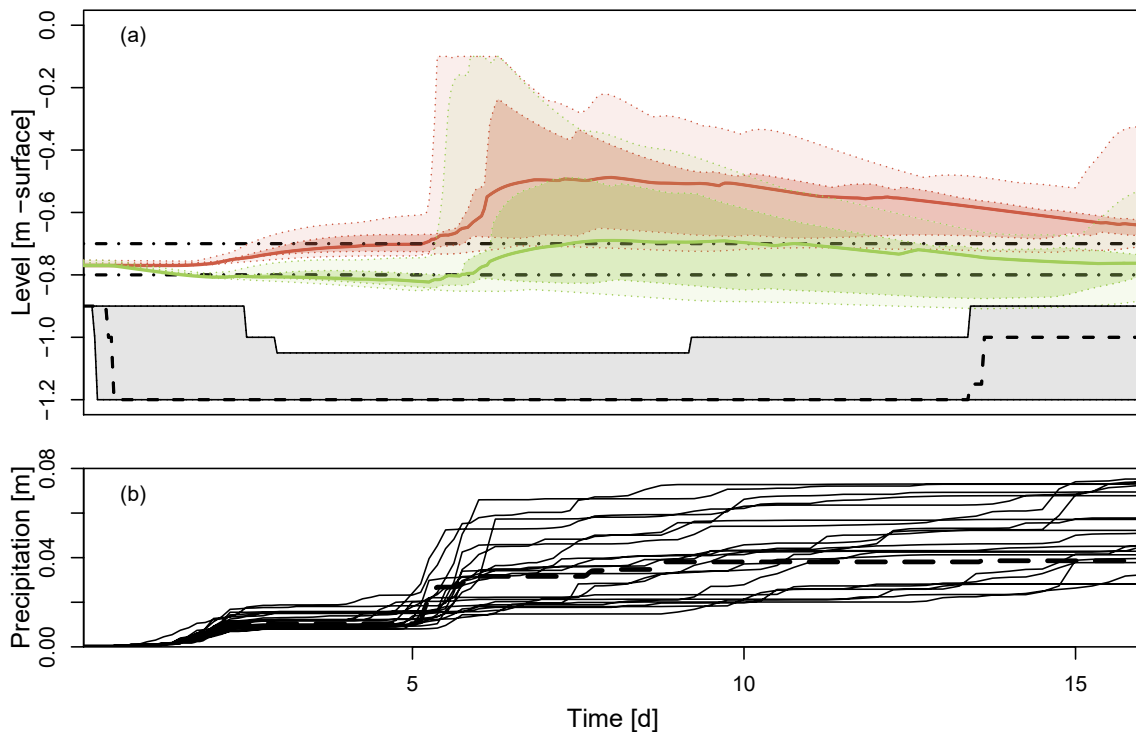


**Figure 6.** (a) Median water level development over time without drainage base changes (red line) and its uncertainty (dark red area: 50th percentile, light red: 100th percentile), median optimal drainage base management strategy (dashed black) and its uncertainty (gray area: 50th percentile), and median water level development using the median optimal drainage base management strategy (green line) and its uncertainty (dark green area: 50th percentile, light green area: 100th percentile). (b) Cumulative precipitation amounts for 21 weather forecast (solid lines), and observation at Schiphol Airport (dashed line).

rather drastical decrease in drainage base is required for most forecasts for water levels to remain within (or as close as possible to) the optimal range. Already on the first day the majority of the weather forecasts requires lowering of the drainage base, despite most significant rain being five days ahead. However, in at least 25% of the forecasts lowering of the drainage base can wait for two days or more, as precipitation amounts in these forecasts are relatively small. It is expected that the drainage base must remain at its lowest position for at least 13 days, before it can be raised again. However, the exact timing of this is, at the moment of this forecast, not so certain and also less relevant as conditions can be reexamined with each new ensemble forecast and with actual observations of groundwater levels following the precipitation event.

The expected water levels midway between the drains when the optimal (median) drainage base management strategy is applied are given in green. The median (solid line), 50th percentile (dark shaded) and extremes (light shaded) are shown. It is evident that by lowering the drainage base in the first day, the expected peak in water level is much smaller than without management of the drainage base. The median of the expected water levels remains within or is close to the optimal range. However, water levels still rise toward soil surface for a few weather forecasts, and for others water levels fall below the optimal range, indicating over-drainage. Groundwater levels also fall below the optimal range prior to the expected rainfall event on day five in most cases, which is required to enlarge the soils storage capacity prior to the rainfall event and to limit extreme increases in water levels. As most forecasts indicate a significant amount of precipitation around day five, it seems quite certain that any over-drainage will be compensated, although the event is still five days ahead. As new weather forecasts become available with time progressing, the drainage base management strategy can be revised with each new forecast. So, in case the expected rain on day five would, after all, not occur, this will likely become evident in the days prior to this event. The drainage base should then be raised once more in order to limit excess discharge of water.

#### 4. Discussion and Conclusion

The analytical model presented in this paper performs well in comparison with simulated groundwater levels and discharge rates of the numerical model SUTRA. Minor differences are (a) a slightly higher steady state head buildup midway between the drains, (b) a misrepresentation of systems with a large entrance resistance, (c) a smaller discharge peak and response time following drainage base lowering, (d) a longer time required for the groundwater table to flatten after a drainage base raise and (e) a slightly earlier yet less intense increase in water levels midway between the drains following a precipitation event.

The first deviation (a) has been recognized in the literature for the steady state model of Hooghoudt (1940) and may be attributed to horizontal flow occurring in the capillary fringe of the unsaturated zone (Shokri & Bardsley, 2015; Yousfi et al., 2014). This leads to an underestimation of the equivalent flow depth ( $D_e$ ), and thus an overestimation of the head difference required to discharge water. Horizontal flow in the unsaturated zone is indeed present in numerical model results. Other factors that influence analytically obtained steady state heads are the assumption that the head above the drain is exactly the same as the head inside the drain, whilst the head above the drain in the numerical model is mostly slightly higher, and the fact that the analytical model neglects both head loss due to vertical flow (i.e., from groundwater level surface to drain depth) as well as radial flow in the region in which head buildup occurs. The latter aspect has been accounted for by an adapted steady state equation by Mishra and Singh (2007), but they found that the effects on calculated water levels midway between the drain were marginal. Deviation (b) cannot be resolved in the current analytical model definition, hence our model is limited to situations where the entrance geometrical resistance factor is lower than 1 ( $\alpha_e < 1$ ). The other deviations (c–e) have, as demonstrated, a limited impact on the overall model result, but might require attention in specific situations. Under normal field circumstances, uncertainty in soil hydraulic parameters, entrance resistance or other parameters are likely to have a larger impact on model results than these model uncertainties, as demonstrated by e.g., Baroni et al. (2010).

The model application shown in this study provides some insight into the possibilities and challenges of anticipatory drainage base management. Based on our example, frequent anticipatory management may be possible with the analytical model presented, but care should be taken with uncertainty in precipitation forecasts. Also, potential benefits of controlled drainage in general, and especially anticipatory management in these drainage systems, are highly dependent on local circumstances and the drainage system layout (Schilling et al., 2015; Stuyt et al., 2005). Based on for instance Figure 3b, not all drain layout combinations are suitable for daily management due to response times of up to 40 days, but many combinations do provide a fast response. Also local (hydrological) circumstances play an important role. For instance, in case groundwater levels only shortly reach above the drain level in winter season, additional water storage due to controlled drainage may be no more than a few millimeters (Rozemeijer et al., 2016). However, additional water storage can be significant in case of (seasonally) high groundwater levels resulting from a precipitation surplus or local seepage, when proper drainage base management is applied to retain this water as buffer for a following dry period.

Drain spacing should not be too wide (resulting in longer response times due to increased soil water volumes) and drain installation depth should not be too shallow (resulting in limited options for management and limited additional water storage) to make optimal use of the possibilities of controlled drainage for anticipatory management (Ross et al., 2016; Skaggs, Fausey, & Evans, 2012). Deeper installation of drains in itself has little influence on the response time of groundwater levels to adapt to changes in the drainage base, but a larger total equivalent flow depth ( $D_e$ ) can be achieved with more deeply installed drains. It follows from (2) and (4) that for a situation with the same groundwater level and aquifer thickness, more deeply installed drains combined with a raised drainage base can provide a larger total equivalent flow depth as compared to the same situation with shallower drains without raised drainage base, as less radial flow resistance is present. A larger total equivalent flow depth in turn results in shorter response times due to a larger transport capacity in the saturated zone and flatter groundwater levels.

Some steps still need to be taken to optimally use the presented model for application in daily operational management of controlled drainage. We recognize that the model should be further expanded by including processes as evapotranspiration, subirrigation and spatially variable seepage or complicating factors as



heterogeneity to increase model applicability. Also, more attention should be given to which weather forecasts and forecast lengths should be used, and how weather forecast uncertainty reflects on the confidence of the produced optimal drainage base management strategy. Especially in case of (predicted) local, but intense summer storms which may or may not reach the field, care should be taken. We therefore recommend further (case) studies into the use and potential benefits of daily anticipatory drainage base management using the presented model, as compared to both normal and seasonally controlled drainage.

## Appendix A: Symbology

**Table A1:** Symbols Used in the Main Body of This Paper, Including Their Unit and Meaning

Type	Symbol	Unit	Meaning
Lower case	$a$	$T^{-1}$	Factor in Hooghoudt equation equal to $8K_s D_e / L^2$
	$b$	$L^{-1} T^{-1}$	Factor in Hooghoudt equation equal to $4K_s / L^2$
	$d_l$	L	Equivalent flow depth below drain
	$d_u$	L	Equivalent flow depth above drain
	$h_u$	L	Pressure head in unsaturated zone
	$m$	L	Head buildup midway between the drains
	$m_0$	L	Head buildup midway between the drains upon lowering drainage base
	$n$	-	Geometrical factor in Van Genuchten function
	$r_e$	L	Effective drain radius, accounting for entrance resistance
	$r_i$	L	Inner drain radius
	$r_o$	L	Radius of drain plus envelope
	$t$	T	Time
	$x$	L	Horizontal coordinate, positive away from the drain
	$\bar{x}$	-	Dimensionless position of $\bar{z}$ on horizontal axis
	$\bar{x}_h$	-	Dimensionless position of $\bar{z}_h$ on horizontal axis
	$\bar{x}_l$	-	Dimensionless position of $\bar{z}_l$ on horizontal axis
	$z$	L	Vertical coordinate, positive upward
	$z_u$	L	Unsaturated zone coordinate with respect to groundwater level, positive upward
	$\bar{z}$	-	Dimensionless average height of ellipse
	$\bar{z}_h$	-	Dimensionless average height of upper half of ellipse
	$\bar{z}_l$	-	Dimensionless average height of lower half of ellipse
	$\bar{z}_l^*$	-	Dimensionless average height of lower half of ellipse, with respect to $\bar{z}$
Upper case	$A$	$T^{-1}$	Factor equal to $\sqrt{a^2 + 4b(R + S)}$
	$B$	$T^{-1}$	Factor equal to $2bm(t) + a$
	$C_d$	-	Drainage resistance factor
	$D$	L	Depth of drains below surface level
	$D_e$	L	Total equivalent flow depth, summation of $d_l$ and $d_u$
	$D_s$	L	Average thickness of saturated zone
	$D_u$	L	Average thickness of unsaturated zone
	$H_d$	L	Pressure head inside the drain, relative to drain position
	$H_0$	L	Water level directly above the drain, relative to drain position
	$K_e$	$LT^{-1}$	Saturated hydraulic conductivity of drain envelope
	$K_s$	$LT^{-1}$	Saturated hydraulic conductivity of soil
	$L$	L	Distance between two parallel drains

**Table A1**  
*Continued*

Type	Symbol	Unit	Meaning
	$P$	$LT^{-1}$	Precipitation rate
	$Q$	$LT^{-1}$	Drain discharge due to head buildup, normalized by $L/2$
	$Q_l$	$L^2T^{-1}$	Leveling flux from higher to lower part, in case of no drainage
	$Q_0$	$LT^{-1}$	Drain discharge due to lowering of the drainage base, normalized by $L/2$
	$R$	$LT^{-1}$	Recharge rate from unsaturated to saturated zone
	$S$	$LT^{-1}$	Seepage rate
	$S_y$	-	Specific yield
	$V_l$	$L^2$	Volume of water in the lower part, in case of no drainage
	$V_s$	$L$	Horizontally averaged volume of water in saturated zone
	$V_u$	$L$	Horizontally averaged volume of water in unsaturated zone
	$Z$	$L$	Depth of low-permeable layer
Greek	$\alpha$	$L^{-1}$	Geometrical factor in Van Genuchten function
	$\alpha_e$	-	Entrance geometrical resistance factor
	$\theta_h$	-	Water content for a given pressure $h_u$
	$\theta_r$	-	Residual water content
	$\theta_s$	-	Water content at saturation

## Appendix B: Equation Derivation

Derivations of head buildup change over time (8) and leveling of the water table after raising the drainage base (11) are provided below. Some additional information on the unsaturated zone Equation 14 is provided as well.

### Appendix B1. Saturated Zone

Under all circumstances we assume that the groundwater level distribution under a situation with positive recharge and seepage follows an elliptical shape, given by

$$\frac{(f-x)^2}{f^2} + \frac{z^2}{g^2} = 1; \quad 0 \leq x \leq \frac{L}{2}; \quad 0 \leq z \leq m \quad (B1)$$

where  $x$  [L] denotes the horizontal position, with  $x = 0$  at the drain and  $x = L/2$  midway between the drains,  $z$  [L] denotes the water level relative to the water level at  $x = 0$ ,  $f$  [L] denotes the maximum length of  $x$ , equal to  $L/2$  and  $g$  [L] denotes the maximum water level, equal to head buildup  $m$ . Integrating this equation over  $x$  and dividing by  $m$  yields the average watertable height,  $\bar{g} = \pi/4g$ , which is the same as the horizontally averaged volume of the saturated part above  $z = -D + H_0$ , given by  $V_s$ . A change in  $V_s$  is related to a change in head buildup, multiplied by specific yield (5). A change in volume itself is the result of an imbalance in in- and outgoing fluxes (6). As the latter is directly related to head buildup midway between the drains through (1), this can be combined to yield (7):

$$S_y \frac{\pi}{4} \int \frac{1}{am + bm^2 - (R + S)} dm = \int -dt \quad (B2)$$

To arrive at (8), this formula is expanded, in analogy of Wesseling (1959), as

$$\frac{\pi S_y}{4b} \int \left( \frac{Fdm}{m - \frac{-a + \sqrt{a^2 - 4b(R+S)}}{2b}} + \frac{Gdm}{m - \frac{-a - \sqrt{a^2 - 4b(R+S)}}{2b}} \right) = \int -dt \quad (\text{B3})$$

$$\text{with } F = \frac{b}{\sqrt{a^2 + 4b(R+S)}} \text{ and } G = \frac{-b}{\sqrt{a^2 + 4b(R+S)}}.$$

Further rewriting and integration of this equation between time  $t = t$  and  $t = t + \Delta t$  yields:

$$\frac{\pi S_y}{4\sqrt{a^2 + 4b(R+S)}} \left[ \ln \left( \frac{2bm + a - \sqrt{a^2 - 4b(R+S)}}{2bm + a + \sqrt{a^2 - 4b(R+S)}} \right) \right]_{m(t=t)}^{m(t=t+\Delta t)} = [-t]_{t=t}^{t=t+\Delta t} \quad (\text{B4})$$

where we implicitly assume that all variables on the left hand side are independent of time. This equation can be rewritten as

$$\frac{2bm(t=t+\Delta t) + a - \sqrt{a^2 + 4b(R+S)}}{2bm(t=t+\Delta t) + a + \sqrt{a^2 + 4b(R+S)}} \frac{2bm(t=t) + a + \sqrt{a^2 + 4b(R+S)}}{2bm(t=t) + a - \sqrt{a^2 + 4b(R+S)}} = \exp \left( -\frac{4\sqrt{a^2 + 4b(R+S)}}{\pi S_y} \Delta t \right) \quad (\text{B5})$$

By defining  $A_1 = \sqrt{a^2 + 4b(R+S)}$ ,  $A_2 = 2bm(t=t) + a$  and  $A_3 = 2bm(t=t+\Delta t) + a$  this equation is simplified to

$$\frac{A_3 - A_1}{A_3 + A_1} \frac{A_2 + A_1}{A_2 - A_1} = \exp \left( -\frac{4 A_1}{\pi S_y} \Delta t \right) \quad (\text{B6})$$

From (1) it follows that  $2bm + a = \sqrt{a^2 + 4b(R+S)}$  for a steady state situation. We also define the water balance such that  $R + S = Q(\text{steady state})$ . For  $A_2$  we can therefore write  $A_2 = 2bm(t=t) + a = \sqrt{a^2 + 4bQ(t=t)}$  and for  $A_3$  we write  $A_3 = 2bm(t=t+\Delta t) + a = \sqrt{a^2 + 4bQ(t=t+\Delta t)}$ . Solving (B6) for  $A_3$  yields a function at time  $t + \Delta t$ :

$$A_3 = \frac{A_1 A_2 + A_1^2 \tanh \left( \frac{2 A_1}{\pi S_y} \Delta t \right)}{A_2 \tanh \left( \frac{2 A_1}{\pi S_y} \Delta t \right) + A_1} = 2bm(t=t+\Delta t) + a = \sqrt{a^2 + 4bQ(t=t+\Delta t)} \quad (\text{B7})$$

Using the final equality in (B7) we either arrive at a function for  $m$  (8) or, alternatively,  $Q$ , when we use  $A_2 = \sqrt{a^2 + 4bQ(t=t)}$  rather than  $A_2 = 2bm(t=t) + a$ :

$$Q(t=t+\Delta t) = \frac{\left( A_1 A_2 + A_1^2 \tanh \left( \frac{2 A_1}{\pi S_y} \Delta t \right) \right)^2}{4b \left( A_2 \tanh \left( \frac{2 A_1}{\pi S_y} \Delta t \right) + A_1 \right)^2} - bD_e^2 \quad (\text{B8})$$

For the derivation of (11) in case the drainage base is raised and discharge ceases, we again use the assumption of the elliptical groundwater shape as given by (B1), with its average height  $g\bar{z} = \pi/4g$ . We divide the ellipse into two zones (see Figure 2b), such that all water from the upper zone can be stored in lower zone

to yield a flat groundwater level profile. The horizontal position at which the separation between the zones is present is at the location where the groundwater level equals the average height, as found by inserting  $g\bar{z}$  into (B1):

$$f - x = \sqrt{\left(1 - \frac{(g\bar{z})^2}{g^2}\right)(f)^2} \rightarrow f\bar{x} = f \left(1 - \sqrt{1 - \left(\frac{\pi}{4}\right)^2}\right) \quad (\text{B9})$$

In a similar fashion, we obtain the average water height and horizontal position at which this average occurs, by integrating each zone over  $x$ , and substituting the result into (B1). For the lower zone, we integrate from  $0 < x < f\bar{x}$ , to obtain  $\bar{z}_l$  as

$$g\bar{z}_l = \frac{1}{f\bar{x}} \int_0^{f\bar{x}} \sqrt{\left(1 - \frac{(f-x)^2}{(f)^2}\right)} g^2 dx = \frac{\pi(1-\bar{x}) - 4\cos^{-1}(1-\bar{x})}{-8\bar{x}} g \quad (\text{B10})$$

and its corresponding horizontal location  $\bar{x}_l$

$$f\bar{x}_l = f \left(1 - \sqrt{1 - \frac{(\pi(1-\bar{x}) - 4\cos^{-1}(1-\bar{x}))^2}{(-8\bar{x})^2}}\right) \quad (\text{B11})$$

For the upper zone, we integrate from  $f\bar{x} < x < f$ , to obtain  $\bar{z}_h$  as

$$g\bar{z}_h = \frac{1}{f - f\bar{x}} \int_{f\bar{x}}^f \sqrt{\left(1 - \frac{(f-x)^2}{(f)^2}\right)} g^2 dx = \frac{\pi(1-\bar{x}) + 4\sin^{-1}(1-\bar{x})}{8(1-\bar{x})} g \quad (\text{B12})$$

and its corresponding horizontal location  $\bar{x}_h$

$$f\bar{x}_h = f \left(1 - \sqrt{1 - \frac{(\pi(1-\bar{x}) + 4\sin^{-1}(1-\bar{x}))^2}{(8(1-\bar{x}))^2}}\right) \quad (\text{B13})$$

If we assume that the flux between two zones is given by a Darcy flux, this flux can be written as the head gradient between the upper and lower zone divided by their distance, multiplied with the hydraulic conductivity and flow depth, such that the leveling flux (9) is given by

$$Q_l = -K_s D_s \frac{(\bar{z}_h - \bar{z}_l)g}{(\bar{x}_h - \bar{x}_l)f} = \frac{K_s D_s g}{(\bar{x}_h - \bar{x}_l)f} \frac{\pi(1-\bar{x}) - 4\sin^{-1}(1-\bar{x})}{(-8\bar{x})^2} = \frac{K_s D_s \bar{z}_l g}{(\bar{x}_h - \bar{x}_l)f (1-\bar{x}) (\pi(1-\bar{x}) - 4\cos^{-1}(1-\bar{x}))} \quad (\text{B14})$$

where  $D_s [L]$  gives the saturated zone thickness at  $x = f\bar{x}$ , equal to  $Z - D + H_0 + g\bar{z}$ . The last equality in (B14) follows from (B10). Using similar assumptions as made in the derivation of (8), we assume that a change in storage in the lower zone, given by  $\Delta V_l [L^2]$  is given by:

$$\Delta V_l = f\bar{x} S_y g \Delta \bar{z}_l \quad (\text{B15})$$

Since the volume in the lower zone can only change by inflow of water from the higher zone, we can state that

$$\frac{\Delta V_l}{\Delta t} = +Q_l = \frac{K_s D_s \bar{z}_l g}{(\bar{x}_h - \bar{x}_l) f (1 - \bar{x}) (\pi(1 - \bar{x}) - 4 \cos^{-1}(1 - \bar{x}))} \frac{\pi(1 - \bar{x}) - 4 \sin^{-1}(1 - \bar{x})}{\pi(1 - \bar{x}) - 4 \cos^{-1}(1 - \bar{x})} \quad (\text{B16})$$

Defining  $\bar{z}_l^* = \bar{z}_l - \bar{z}$ , such that  $\bar{z}_l^*$  is the height of the lower zone with respect to the average height, and combining (B15) and (B16), we obtain

$$\int_{\bar{z}_l^*(t=t)}^{\bar{z}_l^*(t=t+\Delta t)} \frac{1}{\bar{z}_l^*} d\bar{z}_l^* = \frac{K_s D_s}{S_y (\bar{x}_h - \bar{x}_l) f^2} \frac{\pi(1 - \bar{x}) - 4 \sin^{-1}(1 - \bar{x})}{-\bar{x}(1 - \bar{x}) (\pi(1 - \bar{x}) - 4 \cos^{-1}(1 - \bar{x}))} \int_{t=t}^{t=t+\Delta t} dt \quad (\text{B17})$$

which leads to (11)

$$g \bar{z}_l^*(t = t + \Delta t) = \bar{z}_l^*(t = t) g * \exp \left( \frac{K_s D_s \Delta t}{S_y (\bar{x}_h - \bar{x}_l) f^2} \frac{\pi(1 - \bar{x}) - 4 \sin^{-1}(1 - \bar{x})}{-\bar{x}(1 - \bar{x}) (\pi(1 - \bar{x}) - 4 \cos^{-1}(1 - \bar{x}))} \right) \quad (\text{B18})$$

Finally, a change in water level in the lower zone corresponds to a change in both  $H_0$  and  $m$ . Given the elliptical groundwater shape, these can be interchanged, such that the corresponding head buildup  $m$  is given by

$$m(t + \Delta t) = g \bar{z}_l^*(t + \Delta t) \frac{-8\bar{x}}{4 \sin^{-1}(1 - \bar{x}) - \pi(1 - \bar{x})} \quad (\text{B19})$$

and the water level at  $x = 0$  is given by

$$H_0(t + \Delta t) = H_0(t) + \bar{z} (g - m(t + \Delta t)) \quad (\text{B20})$$

## Appendix B2. Unsaturated Zone

For the derivation of (14), we start from the definitions of the unsaturated zone as given by the van Genuchten (1980) functions and provided in Voss and Provost (2002):

$$\theta_h = \theta_r + (\theta_s - \theta_r) \left( 1 + (\alpha |h_u|)^n \right)^{\frac{1-n}{n}} \quad (\text{B21})$$

$$\theta^* = \frac{\theta_h - \theta_r}{\theta_s - \theta_r} \quad (\text{B22})$$

$$K_r = \sqrt{\theta^*} \left( 1 - \left( 1 - \theta^{*\frac{n}{n-1}} \right)^{\frac{n-1}{n}} \right)^2 \quad (\text{B23})$$

where  $K_r[-]$  is the hydraulic conductivity relative to saturated conductivity  $K_s$  and  $\theta^*[-]$  is the relative water content. Other symbols are defined in Appendix A.

Combining (B21) and (B22) yields a direct relation between relative water content and pressure head as

$$\theta^* = \frac{\theta_r + (\theta_s - \theta_r) \left( 1 + (\alpha |h_u|)^n \right)^{\frac{1-n}{n}} - \theta_r}{\theta_s - \theta_r} = \left( 1 + (\alpha |h_u|)^n \right)^{\frac{1-n}{n}} \quad (\text{B24})$$

and combining this with (B23) yields a relation between relative hydraulic conductivity and pressure head

$$K_r = \left(1 + (\alpha |h_u|)^n\right)^{\frac{1-n}{2n}} \left[1 - \left(1 - \left(1 + (\alpha |h_u|)^n\right)^{\frac{1-n}{n-1}}\right)^{\frac{n-1}{n}}\right]^2 \quad (\text{B25})$$

Realizing that  $\left(x^{\frac{1-n}{n}}\right)^{\frac{n}{n-1}} = \frac{1}{x}$ , we rewrite  $K_r$  accordingly

$$K_r = \left(1 + (\alpha |h_u|)^n\right)^{\frac{1-n}{2n}} \left[1 - \frac{1}{1 + (\alpha |h_u|)^n}\right]^{\frac{n-1}{n}} \quad (\text{B26})$$

To obtain the change in pressure head within a finite vertical distance in the unsaturated zone for any given flux rate, we use the Darcy equation for vertical flow, given by

$$q = -K \frac{dH}{dz_u} = -K \frac{d(h_u + z_u)}{dz_u} \quad (\text{B27})$$

We may rewrite this to obtain the change in pressure head with a change in vertical position as

$$dh_u = \left(-\frac{q}{K_s K_r} - 1\right) dz_u = \frac{-q - K_s K_r}{K_s K_r} dz_u \quad (\text{B28})$$

Substitution of  $q = -R$  to account for the fact that  $R$  is defined positive into the groundwater (which is a downward direction with respect to the unsaturated zone) whereas  $q$  is defined positive in the positive vertical direction, and substitution of (B26) for  $K_r$ , yields (14). Alternatively, (B23) may be substituted to yield an expression as function of relative water content as

$$dh_u = \frac{R - K_s \left(1 + (\alpha |h_u|)^n\right)^{\frac{1-n}{2n}} \left[1 - \frac{1}{1 + (\alpha |h_u|)^n}\right]^{\frac{n-1}{n}}}{K_s \left(1 + (\alpha |h_u|)^n\right)^{\frac{1-n}{2n}} \left[1 - \frac{1}{1 + (\alpha |h_u|)^n}\right]^{\frac{n-1}{n}}} dz_u = \frac{R - K_s \sqrt{\theta^*} \left[1 - \left(1 - \theta^{*\frac{n}{n-1}}\right)^{\frac{n-1}{n}}\right]^2}{K_s \sqrt{\theta^*} \left[1 - \left(1 - \theta^{*\frac{n}{n-1}}\right)^{\frac{n-1}{n}}\right]^2} dz_u \quad (\text{B29})$$

## Data Availability Statement

Source code and data related to this publication is available for download from <http://doi.org/10.5281/zenodo.4428869> (van de Craats et al., 2021).

## References

- Appels, W. M., Bogaart, P. W., & van der Zee, S. E. A. T. M. (2017). Feedbacks between shallow groundwater dynamics and surface topography on runoff generation in flat fields. *Water Resources Research*, 53, 10336–10353. <https://doi.org/10.1002/2017WR020727>
- Baroni, G., Facchi, A., Gandolfi, C., Ortuani, B., Horeschi, D., & van Dam, J. C. (2010). Uncertainty in the determination of soil hydraulic parameters and its influence on the performance of two hydrological models of different complexity. *Hydrology and Earth System Sciences*, 14(2), 251–270. <https://doi.org/10.5194/hess-14-251-2010>

## Acknowledgments

This research in the context of the project Water Nexus is financed by the Netherlands Organisation for Scientific Research (NWO) under Contract no. 14299, which is partly funded by the Ministry of Economic Affairs and Climate Policy, and co-financed by the Netherlands Ministry of Infrastructure and Water Management and partners of the Dutch Water Nexus consortium.



- Bento, C. P. M., Commelin, M. C., Baartman, J. E. M., Yang, X., Peters, P., Mol, H. G. J., et al. (2018). Spatial glyphosate and AMPA redistribution on the soil surface driven by sediment transport processes – A flume experiment. *Environmental Pollution*, 234, 1011–1020. <https://doi.org/10.1016/j.envpol.2017.12.003>
- Campolongo, F., Cariboni, J., & Saltelli, A. (2007). An effective screening design for sensitivity analysis of large models. *Environmental Modelling & Software*, 22(10), 1509–1518. <https://doi.org/10.1016/j.envsoft.2006.10.004>
- Cooke, R. A., Badiger, S., & Garcia, A. M. (2001). Drainage equations for random and irregular tile drainage systems. *Agricultural Water Management*, 48(3), 207–224. [https://doi.org/10.1016/S0378-3774\(00\)00136-0](https://doi.org/10.1016/S0378-3774(00)00136-0)
- Ernst, L. F. (1956). Calculation of the steady flow of groundwater in vertical cross-sections. *Netherlands Journal of Agricultural Science*, 4, 126–131. <https://doi.org/10.18174/njas.v4i1.17793>
- Ernst, L. F. (1962). Grondwaterstromingen in de verzadigde zone en hun berekening bij de aanwezigheid van horizontale evenwijdige open leidingen. [Groundwater flow in the saturated zone and its calculation when parallel horizontal open conduits are present]. *Verslagen van Landbouwkundige Onderzoekingen*, 67(15), 189.
- Geuzaine, C., & Remacle, J. F. (2009). Gmsh: A 3-D finite element mesh generator with built-in pre- and post-processing facilities. *International Journal for Numerical Methods in Engineering*, 79(11), 1309–1331. <https://doi.org/10.1002/nme.2579>
- Hooghoudt, S. B. (1940). Algemeene beschouwing van het probleem van de detailontwatering en de infiltratie door middel van parallel loopende drains, greppels, slooten en kanalen. [General consideration of the problem of drainage and infiltration using parallel tile drains, surface drains, ditches and canals]. *Verslagen van Landbouwkundige Onderzoekingen*, 46(14), 515–707.
- Karandish, F., Darzi-Naftchali, A., & Šimůnek, J. (2018). Application of HYDRUS (2D/3D) for predicting the influence of subsurface drainage on soil water dynamics in a rainfed-canola cropping system. *Irrigation and Drainage*, 67(S2), 29–39. <https://doi.org/10.1002/ird.2194>
- Kirkham, D. (1958). Seepage of steady rainfall through soil into drains. *EOS Transactions American Geophysical Union*, 39(5), 892–908. <https://doi.org/10.1029/TR039i005p00892>
- KNMI. (2019). Royal Netherlands Meteorological Institute (KNMI). Retrieved from <https://www.knmi.nl/nederland-nu/klimatologie/uurgegevens>
- Kraijenhoff van de Leur, D. A. (1958). A study of non-steady groundwater flow with special reference to a reservoir-coefficient. *De Ingenieur*, 70(19), 87–94.
- Mishra, G. C., & Singh, V. (2007). A new drain spacing formula. *Hydrological Sciences Journal*, 52(2), 338–351. <https://doi.org/10.1623/hysj.52.2.338>
- Morris, M. D. (1991). Factorial sampling plans for preliminary computational experiments. *Technometrics*, 33(2), 161–174. <https://doi.org/10.1080/00401706.1991.10484804>
- Ritzema, H. P., & van Loon-Steensma, J. M. (2017). Coping with climate change in a densely populated delta: A paradigm shift in flood and water management in the Netherlands. *Irrigation and Drainage*, 67(S1), 52–65. <https://doi.org/10.1002/ird.2128>
- Ross, J. A., Herbert, M. E., Sowa, S. P., Frankenberger, J. R., King, K. W., Christopher, S. F., et al. (2016). A synthesis and comparative evaluation of factors influencing the effectiveness of drainage water management. *Agricultural Water Management*, 178, 366–376. <https://doi.org/10.1016/j.agwat.2016.10.011>
- Rowell, D. P. (2009). Projected midlatitude continental summer drying: North America versus Europe. *Journal of Climate*, 22(11), 2813–2833. <https://doi.org/10.1175/2008JCLI2173.1>
- Rozemeijer, J. C., Visser, A., Borren, W., Winegram, M., van der Velde, Y., Klein, J., & Broers, H. P. (2016). High-frequency monitoring of water fluxes and nutrient loads to assess the effects of controlled drainage on water storage and nutrient transport. *Hydrology and Earth System Sciences*, 20(1), 347–358. <https://doi.org/10.5194/hess-20-347-2016>
- Schilling, K. E., Wolter, C. F., Isenhardt, T. M., & Schultz, R. C. (2015). Tile drainage density reduces groundwater travel times and compromises riparian buffer effectiveness. *Journal of Environmental Quality*, 44(6), 1754–1763. <https://doi.org/10.2134/jeq2015.02.0105>
- Schott, L., Lagzdins, A., Daigh, A., Craft, K., Pederson, C., Brenneman, G., & Helmers, M. (2017). Drainage water management effects over five years on water tables, drainage, and yields in southeast Iowa. *Journal of Soil and Water Conservation*, 72(3), 251–259. <https://doi.org/10.2489/jswc.72.3.251>
- Shokri, A., & Bardsley, W. E. (2015). Enhancement of the Hooghoudt drain-spacing equation. *Journal of Irrigation and Drainage Engineering*, 141(6), 04014070. [https://doi.org/10.1061/\(ASCE\)IR.1943-4774.0000835](https://doi.org/10.1061/(ASCE)IR.1943-4774.0000835)
- Skaggs, R. W., Fausey, N. R., & Evans, R. O. (2012). Drainage water management. *Journal of Soil and Water Conservation*, 67(6), 167A–172A. <https://doi.org/10.2489/jswc.67.6.167A>
- Skaggs, R. W., Youssef, M., & Chescheir, G. M. (2012). DRAINMOD: Model use, calibration, and validation. *Transactions of the ASABE*, 55, 1509–1522. <https://doi.org/10.13031/2013.42259>
- Sloan, B. P., Basu, N. B., & Mantilla, R. (2016). Hydrologic impacts of subsurface drainage at the field scale: Climate, landscape and anthropogenic controls. *Agricultural Water Management*, 165, 1–10. <https://doi.org/10.1016/j.agwat.2015.10.008>
- Smedema, L. K., Vlotman, W. F., & Rycroft, D. W. (2004). *Modern land drainage: Planning, design and management of agricultural drainage systems* (p. 449). London: Taylor & Francis.
- Spinoni, J., Vogt, J. V., Naumann, G., Barbosa, P., & Dosio, A. (2018). Will drought events become more frequent and severe in Europe? *International Journal of Climatology*, 38(4), 1718–1736. <https://doi.org/10.1002/joc.5291>
- Stuyt, L. C. P. M., Dierickx, W., & Martínez Beltrán, J. (2005). *Materials for subsurface land drainage systems*. Rome: Food & Agriculture Org.
- Sunohara, M. D., Gottschall, N., Craiovan, E., Wilkes, G., Topp, E., Frey, S. K., & Lapen, D. R. (2016). Controlling tile drainage during the growing season in Eastern Canada to reduce nitrogen, phosphorus, and bacteria loading to surface water. *Agricultural Water Management*, 178, 159–170. <https://doi.org/10.1016/j.agwat.2016.08.030>
- van der Craats, D., van der Zee, S. E. A. T. M., & Leijnse, A. (2021). Anticipatory drainage base management for groundwater level optimization [Data Set]. *Zenodo*. <https://doi.org/10.5281/zenodo.4428869>
- van der Molen, W. H., Martínez Beltrán, J., & Ochs, W. J. (2007). *Guidelines and computer programs for the planning and design of land drainage systems* (Vol. 62). Rome: Food & Agriculture Org.
- van der Zee, S. E. A. T. M., Stoffberg, S. F., Yang, X., Liu, Y., Islam, M. N., & Hu, Y. F. (2017). Irrigation and drainage in agriculture: A salinity and environmental perspective. In S. Kulshreshtha, & A. Elshorbagy (Eds.), *Current perspective on irrigation and drainage*. <https://doi.org/10.5772/66046>
- van Genuchten, M. (1980). A closed-form equation for predicting the hydraulic conductivity of unsaturated soils. *Soil Science Society of America Journal*, 44(5), 892–898. <https://doi.org/10.2136/sssaj1980.03615995004400050002x>
- Voss, C. I., & Provost, A. M. (2002). *SUTRA, a model for saturated-unsaturated variable-density groundwater flow with solute or energy transport (version september 22, 2010)* (No. Report 02-4231 (p. 291)). US Geological Survey, Water Resources Investigations.

- Wang, Z., Shao, G., Lu, J., Zhang, K., Gao, Y., & Ding, J. (2020). Effects of controlled drainage on crop yield, drainage water quantity and quality: A meta-analysis. *Agricultural Water Management*, 239, 106253. <https://doi.org/10.1016/j.agwat.2020.106253>
- Wesseling, J. (1959). *Vergelijking voor de niet-stationaire afvoer* [equation for non-stationary discharge]. Nota No. 44 (p. 12). ICW.
- Williams, M. R., King, K. W., & Fausey, N. R. (2015). Drainage water management effects on tile discharge and water quality. *Agricultural Water Management*, 148, 43–51. <https://doi.org/10.1016/j.agwat.2014.09.017>
- Xin, P., Yu, X., Lu, C., & Li, L. (2016). Effects of macro-pores on water flow in coastal subsurface drainage systems. *Advances in Water Resources*, 87, 56–67. <https://doi.org/10.1016/j.advwatres.2015.11.007>
- Youngs, E. G. (1985). A simple drainage equation for predicting water-table drawdowns. *Journal of Agricultural Engineering Research*, 31(4), 321–328. [https://doi.org/10.1016/0021-8634\(85\)90108-8](https://doi.org/10.1016/0021-8634(85)90108-8)
- Yousfi, A., Mecherghi, M., & Ritzema, H. (2014). A drain-spacing equation that takes the horizontal flow in the unsaturated zone above the groundwater into account. *Irrigation and Drainage*, 63(3), 373–382. <https://doi.org/10.1002/ird.1821>
- Youssef, M. A., Abdelbaki, A. M., Negm, L. M., Skaggs, R., Thorp, K. R., & Jaynes, D. B. (2018). DRAINMOD-simulated performance of controlled drainage across the U.S. Midwest. *Agricultural Water Management*, 197, 54–66. <https://doi.org/10.1016/j.agwat.2017.11.012>
- Zhou, X., Zhu, Y., Hou, D., Luo, Y., Peng, J., & Wobus, R. (2017). Performance of the new NCEP global ensemble forecast system in a parallel experiment. *Weather and Forecasting*, 32(5), 1989–2004. <https://doi.org/10.1175/WAF-D-17-0023.1>